Components of a "Dynein Regulatory Complex" Are Located at the Junction between the Radial Spokes and the Dynein Arms in *Chlamydomonas* Flagella

Lynne C. Gardner,* Eileen O'Toole,‡ Catherine A. Perrone,* Thomas Giddings,‡ and Mary E. Porter*

*Department of Cell Biology and Neuroanatomy, University of Minnesota Medical School, Minneapolis, Minnesota 55455; and ‡Department of Molecular, Cellular, and Developmental Biology, University of Colorado at Boulder, Boulder, Colorado 80309-0347

Abstract. Previous studies of flagellar mutants have identified six axonemal polypeptides as components of a "dynein regulatory complex" (DRC). The DRC is thought to coordinate the activity of the multiple flagellar dyneins, but its location within the axoneme has been unknown (Huang et al., 1982; Piperno et al., 1992). We have used improved chromatographic procedures (Kagami and Kamiya, 1992) and computer averaging of EM images (Mastronarde et al., 1992) to analyze the relationship between the DRC and the dynein arms. Our results suggest that some of the DRC components are located at the base of the second radial spoke in close association with the inner dynein arms. (*a*) Averages of axoneme cross-sections indicate that inner arm structures are significantly reduced in three DRC mutants (*pf3*<*pf2*<*sup-pf-3*<*wt*). (*b*) These defects are more pronounced in distal/medial regions of the axoneme than in proximal regions. (*c*) Analysis of flagellar extracts by fast protein liquid chromatography and SDS-PAGE indicates that a specific dynein I2 isoform is missing in *pf3* and reduced in *pf2* and *sup-pf-3*. Comparison with *ida4* and *pf3ida4* extracts reveals that this isoform differs from those missing in *ida4*. (*d*) When viewed in longitudinal section, all three DRC mutants lack a crescent-shaped density above the second radial spoke, and *pf3* axonemes lack additional structures adjacent to the crescent. We propose that the crescent corresponds in part to the location of the DRC, and that this structure is also directly associated with a subset of the inner dynein arms. This position is appropriate for a complex that is thought to mediate signals between the radial spokes and the dynein arms.

THE dynein ATPases are a family of motor proteins that drive microtubule sliding in cilia and flagella and contribute to other forms of microtubule-based motility inside cells. In cilia and flagella, these enzymes form the inner and outer arm structures on the outer doublet microtubules of the axoneme. The study of flagellar mutants in *Chlamydomonas* has clearly established that although the inner and outer arms share a similar structural motif, they are each composed of a distinct set of heavy (>400 kD), intermediate, and light chain polypeptides (Piperno and Luck, 1979; Huang et al., 1979). The outer dynein arm is relatively simple; three heavy chains (α, β, and γ) are associated with two intermediate and several light chains to form a three-headed structure that repeats every 24 nm along the length of the axoneme (Witman et al., 1983; Goodenough and Heuser, 1984). In contrast, the polypeptides of the inner arm dyneins form several different isoforms whose arrangement is complex and may vary from proximal to distal regions of the axoneme (Piperno et al., 1990; Piperno and Raminis, 1991). Early models of inner arm organization suggested that the inner dynein arms are composed of three distinct subunits (I1, I2, and I3), each containing two heavy chains, that repeat in groups of three every 96 nm in register with the radial spokes (Goodenough and Heuser, 1989; Piperno et al., 1990). Subsequent studies have confirmed that the I1 isoform is a discrete two-headed species located at the proximal end of the 96-nm axoneme repeat (Smith and Sale, 1991; Porter et al., 1992; Mastronarde et al., 1992). However, the I2 and I3 isoforms have now been resolved into at least six distinct heavy chain subspecies using improved chromatographic procedures (Kagami and Kamiya, 1992). In addition, recent electron microscopic studies have revealed that the arrangement of structures in the inner arm region is much more complex than previously realized (Muto et al., 1991; Mastronarde et al., 1992). This increased complexity has indicated the necessity for revision in current models of inner arm organization.

The study of flagellar mutants has further demonstrated

Address all correspondence to M. E. Porter, Department of Cell Biology and Neuroanatomy, 4-135 Jackson Hall, 321 Church St. SE, Minneapolis, Minnesota 55455. Ph.: (612) 626-1901. Fax: (612) 624-8118.

that the inner and outer dynein arms have different functions in the generation of flagellar motility (Mitchell and Rosenbaum, 1985; Kamiya, 1988; Brokaw and Kamiya, 1987). While the outer arms add power to the flagellar beat, the inner dynein arms are both necessary and sufficient to generate the ciliary and flagellar waveforms. Measurements of microtubule sliding velocities in vitro also indicate that inner and outer dynein arms drive microtubule translocation at very different intrinsic speeds (Kurimoto and Kamiya, 1991). In addition, both the inner and outer dynein arms can only generate force in a single direction along a microtubule (Sale and Satir, 1977; Fox and Sale, 1987). To work together efficiently, these multiple dynein motors must be selectively activated and inhibited at different points in the flagellar beat cycle, both around the axoneme and along its length. Thus precise spatial and temporal regulation of the multiple dynein motors is required to coordinate microtubule sliding into flagellar bending.

Several lines of structural and genetic evidence implicate the central pair/radial spoke structures as key regulators of dynein arm activity (reviewed in Smith and Sale, 1994). For instance, mutations that disrupt either the central pair microtubules or the radial spokes result in flagellar paralysis (Witman et al., 1978) by a mechanism that appears to involve a global inactivation of dynein arm activity (Huang et al., 1982; Smith and Sale, 1992*a*). The mutant axonemes can still be induced to undergo sliding disintegration in vitro (Witman et al., 1978), but at significantly slower rates than observed with wild-type axonemes (Smith and Sale, 1992*a*). Reconstitution experiments suggest that these changes in sliding velocities may be mediated by posttranslational modifications of the dyneins (Smith and Sale, 1992*a*). This work implies that signals from the central pair/radial spoke complex activate dynein-driven microtubule sliding (Smith and Sale, 1992). Furthermore, in the absence of these signals, other components within the axoneme must inhibit dynein activity.

The presence of such an inhibitory control system within the axoneme has also been indicated by the isolation and characterization of a second group of flagellar mutations. These mutations are extragenic suppressors that restore motility to paralyzed central pair/radial spoke defective mutants without restoring the original missing structures (Huang et al., 1982). By modifying other axonemal components, the suppressor mutations are thought to short circuit or bypass the inhibitory control system and allow for some dynein arm activity in the absence of signals from the central pair/radial spoke complex. The second-site suppressor mutations therefore identify other elements in the signaling pathway between the radial spokes and the dynein arms, including components of the control system, as well as regulatory domains within the dynein arms themselves. In central pair and radial spoke mutants, the control system inhibits dynein arm activity, but in wild-type cells, local and transient interactions between the central pair/radial spoke complex and the control system are presumed to allow selective and coordinated dynein arm activity (Huang et al., 1982).

One group of extragenic suppressors (*pf2*, *pf3*, *sup-pf-3*, *sup-pf-4*, *sup-pf-5*) shares overlapping defects in a subset of six axonemal polypeptides known as the radial spoke specific control system or more recently as the dynein regulatory complex (DRC)[1] (Huang et al., 1982; Piperno et al., 1992). These polypeptides were shown to be tightly associated with the outer doublet microtubules in wild-type axonemes, but their structural location was not identified (Huang et al., 1982). Subsequent analysis of the motility phenotypes of the *pf2* and *pf3* strains revealed similarities with inner arm defective mutants, but the biochemical basis of these defects remained obscure (Brokaw and Kamiya, 1987). More recent studies have suggested that there might be defects in the phosphorylation of inner arm polypeptides in some of the DRC mutants (Luck and Piperno, 1989). In addition, electron microscopic examination of *pf2* axonemes with image averaging techniques has identified a unique structural defect in the inner arm region; *pf2* axonemes lack a crescent-shaped structure located above the second radial spoke (Mastronarde et al., 1992). However, since that work was completed, quantitative electrophoretic studies have indicated that *pf2* axonemes are also partially deficient in I2/I3 inner arm subunits (Piperno et al., 1992).

With the realization that the DRC mutants contain several different kinds of polypeptide defects, it became apparent that we needed to reexamine these strains with improved biochemical and structural techniques. In particular, we wished to identify the specific dynein isoforms that are altered in these mutants, and to analyze their structural relationship with respect to the position of the dynein regulatory complex. In this study, we have used improved fast protein liquid chromatography (FPLC) ion exchange chromatography (Kagami and Kamiya, 1992) to identify the specific inner arm heavy chain defects in the DRC mutants. This work was performed in parallel with quantitative electron microscopy (Mastronarde et al., 1992), which served to localize the protein defects in both cross-sectional and longitudinal views of the axoneme. The use of specific morphological markers also allowed us to find differences in the proximal versus distal distribution of these defects. These studies have identified a structure that is appropriately positioned to mediate local signals between the radial spokes and dynein arms, as well as a subset of inner arm isoforms that appear to be physically associated with components of the DRC. Our results therefore provide new insights into the three-dimensional organization of both the inner dynein arms and the dynein regulatory complex that modulates dynein activity.

Materials and Methods

Mutant Strains

All strains used in this study are listed in Table I. *pf2* and *pf3* were first isolated as motility mutants by R. Lewin and were subsequently shown to have suppressor activity (Huang et al., 1982). *sup-pf-3* and *sup-pf-4* were isolated as extragenic suppressors of paralyzed radial spoke defective strains (Huang et al., 1982). *ida4* is an inner arm mutant that lacks three I2 isoforms (Kagami and Kamiya, 1992) and was generously provided by R. Kamiya (Tokyo University, Tokyo, Japan). The double mutant *pf3 ida4* was constructed in our laboratory using standard techniques.

1. *Abbreviations used in this paper*: DRC, dynein regulatory complex; FPLC, fast protein liquid chromatography; PVDF, polyvinylidene difluoride.

Table I. Characteristics of Mutant Strains Used in This Study

Strain	Motility phenotype	Swimming velocity	Polypeptide defects
		(μm/s)	
wild-type (137c)	wild-type	200.4 ± 16.6	
pf28 (oda2)	slow swimming	ND	Outer arm subunits (*)
ida4-1	abnormal waveform	63.4 ± 11.3	Three I2 isoforms (●)
pf3	abnormal waveform, *pf* suppressor	105.6 ± 11.4	DRC components #1-2 & 5-6 (◇) I2/I3 isoforms reduced ~47% (▽)
pf2	abnormal waveform, *pf* suppressor	73.8 ± 8.4	DRC components #3-7 (◇, $) I2/I3 isoforms reduced ~15% (▽)
sup-pf-3	wild-type motion, *pf* suppressor	119.6 ± 18.6	DRC components #3-6 reduced (◇, ▽) I2/I3 isoforms reduced ~19% (▽)
sup-pf-4	wild-type motion, *pf* suppressor	190.2 ± 11.8	DRC components #5-6 (◇)
pf3 ida4	abnormal waveform, very slow motion	54.4 ± 7.2	DRC components #1-2 & 5-6 (◇) I2 isoforms absent (▽) I3 isoforms reduced (▽)

The motility phenotypes of the DRC mutants were previously described by Brokaw et al., 1982; Brokaw and Luck, 1985; and Brokaw and Kamiya, 1987. Swimming velocities were measured in this study after overnight suspension in liquid media ($N = 20$). The polypeptide defects for each mutant were previously identified by: (*) Mitchell and Rosenbaum, 1985; (●) Kagami and Kamiya, 1992; (◇) Huang et al., 1982; (▽) Piperno et al., 1992; and ($) Piperno et al., 1994.

Cell Culture

Cells were maintained as vegetatively growing cultures at 21°C on rich medium containing sodium acetate, as described by Sager and Granick (1953) and modified by Holmes and Dutcher (1989). Cultures of gametic cells were obtained by transferring strains to a low-sulphate medium for 5–7 d. All solid media contained Bacto agar (Difco Laboratories, Detroit, Michigan) that was washed five times with Milli-Q filtered water and air dried prior to use. The medium for large scale (>5 liters) liquid culture was supplemented with additional potassium phosphate as described by Witman (1986).

Motility Measurements

Measurements of swimming velocities were made from video recordings (BC-1000 VCR; Mitsubishi Electric Sales of America, Cypress, CA) of live cells using a C2400 Newvicon camera and an Argus 10 video processor (Hamamatsu Photonic Systems Corporation, Bridgewater, NJ) calibrated with a stage micrometer.

Protein Purification

Whole axonemes were obtained from small scale cultures of gametic cells on solid medium. The cells were resuspended in minimal medium, allowed to generate flagella for 15–30 min, and collected by centrifugation. Some strains (e.g., *pf3 ida4*) were resuspended in 10 mM Hepes, pH 7.6, to generate flagella. Cells were washed free of debris and cell wall material by two cycles of resuspension and centrifugation in minimal medium, resuspended in 10 mM Hepes, pH 7.4, 1 mM $SrCl_2$, 4% sucrose and 1 mM DTT, and then deflagellated by pH shock (Luck et al., 1977). The solution of deflagellated cells was then supplemented to 5 mM $MgSO_4$, 1 mM EGTA, 0.1 mM EDTA, and 2.5 mg/ml aprotinin, leupeptin, and pepstatin and centrifuged at 1,000 *g*. The supernatant containing flagella was removed, and recentrifuged twice with a 20% sucrose cushion to trap any remaining cell bodies or debris. The clarified flagella were extracted with 0.1% NP-40, and the axonemes were collected by centrifugation at 35,000 *g* for 60 min. The axoneme pellet was then resuspended in NaCl wash buffer (30 mM Hepes, pH 7.4, 5 mM $MgSO_4$, 1 mM EGTA, 0.1 mM EDTA, 25 mM NaCl, 1 mM DTT, and 2. 5 mg/ml aprotinin, leupeptin, and pepstatin), split into two aliquots, and recentrifuged at 14,000 *g* to obtain parallel samples for SDS-PAGE analysis and electron microscopy.

Purified dyneins were prepared from large scale cultures (20–40 liters) of vegetative cells using a modification of procedures described by Witman (1986) and King et al. (1986). Cells were collected using a Pellicon cell harvester (Millipore Corporation, Bedford, MA) equipped with Durapore filter cassettes, and then washed and deflagellated as described above. The final supernatant of clarified flagella was collected directly by centrifugation, resuspended in wash buffer, stripped of flagellar membranes by extraction in 1% NP-40, washed two to three times to remove the detergent, and then extracted in wash buffer containing 0.6 M NaCl, 0.1 mM ATP, and 10 mM taxol for 30 min. The dynein-containing supernatant was collected after centrifugation at 30,000 *g* for 30 min and immediately prepared for analysis by FPLC.

Ion Exchange Chromatography and Nomenclature of Inner Arm Dynein Isoforms

Separation of dynein extracts by ion exchange chromatography was performed as described by Goodenough et al. (1987) with modifications by Kagami and Kamiya (1992). All procedures for dynein fractionation were carried out at 4°C. Chromatography was performed at a flow rate of 1.5 ml/min on a MonoQ HR5/5 analytical anion exchange column (Pharmacia Biotech, Inc., Piscataway, NJ). The dynein-containing extract (0.5–1 mg total protein) was diluted in 9 vol of chromatography buffer (20 mM Hepes pH 7.4, 10 mM NaCl, 5 mM $MgSO_4$, 1 mM DTT, and 1 mg/ml leupeptin) and immediately loaded onto an equilibrated column. The column was briefly washed with buffer containing 100 mM NaCl and then eluted with a linear 100–400 mM NaCl gradient applied over 40 ml. Fractions of 0.5 ml were collected and analyzed by SDS-PAGE.

These conditions produced FPLC profiles of dynein extracts similar to those described by Kagami and Kamiya (1992). Seven peaks containing eight inner arm dynein heavy chains could be identified (see Figs. 1 and 2). To confirm the identity of each dynein subspecies, protein peaks isolated from the outer arm mutant *pf28* were subjected to vanadate cleavage. Each peak produced a unique pattern of cleavage products (Kagami and Kamiya, 1992; and data not shown). We therefore identify the individual inner arm isoforms as subspecies *a–g*, based on their order of elution during ion exchange chromatography and in keeping with the nomenclature of Kagami and Kamiya (1992) and Kato et al. (1993).

Fractions covering the entire profile for each mutant were analyzed at stoichiometric loadings to assess whether or not certain subspecies might be reduced relative to wild-type. Although it was not possible to obtain quantitative measurements from silver stained gels, the elution profiles were reproducible enough to make limited, qualitative comparisons between strains. This was done by examining the total number of fractions over which a specific heavy chain was visible on SDS-gels of the whole FPLC profile and by comparing the staining intensity of fractions that were loaded at the same stoichiometry. For example, subspecies *a*, *b*, and *c* elute as three distinct peaks (A, B, and C) that span at least six fractions apiece and peak four to five fractions apart. Each peak contains a major heavy chain band similar in intensity to the major band in the other two peaks. One can compare peaks A, B, and C relative to one another in a given mutant and with respect to wild-type to get a qualitative impression on the relative abundance of a given peak. On the other hand, peaks D and E are composed

of two asymmetrically eluting heavy chains (subspecies *d* and *e*) that each cover seven fractions and peak only two to three fractions apart. Because the two heavy chains can be resolved on SDS-gels, both bands are visible in peaks D and E (see Fig. 2). However, in an outer arm background, these two subspecies elute as a shoulder on the larger peak of the α/β outer arm complex. To resolve the heavy chains under these conditions, it is necessary to load peaks D, E, and α/β at a lower stoichiometry than peaks A, B, and C. Peaks F and G follow the α/β complex, but contain heavy chains that are easily resolved from one another. Subspecies *f* corresponds to the I1 inner arm complex and contains two heavy chains (1α and 1β). Subspecies *g* contains a single heavy chain species that elutes as a shoulder (peak G) on the trailing edge of peak F.

Sucrose Density Gradient Centrifugation

Purified dyneins were isolated from large scale cultures as described above except that a K-acetate wash buffer (10 mM Hepes, pH 7.4, 5 mM $MgSO_4$, 1 mM DTT, 0.5 mM EGTA, 25 mM potassium acetate, and 1 mg/ml leupeptin) was used to process the axonemes, and the salt extraction was performed using 0.6 M KCl. The high-speed supernatant was dialyzed against K-acetate buffer for 24 h, centrifuged at 30,000 *g* for 30 min and loaded onto a 5–20% sucrose density gradient (13 ml). The gradients were centrifuged in a SW41 rotor (Beckman Instruments, Palo Alto, CA) for 14 h at 33,500 rpm, collected into 0.75 ml fractions, and then analyzed by ATPase assays and SDS-PAGE. Under these conditions, most of the γ heavy chain cosediments with the α and β heavy chains of the outer arm complex at 23 S, and the I2 and I3 inner arm isoforms sediment as a broad peak around 11–12 S (Takada et al., 1992). Fractions surrounding the 11–12 S peak were pooled and further fractionated by FPLC.

Biochemical Analysis

The ATPase activity of whole axonemes, high salt extracts, and extracted outer doublets was measured in the presence of 0.3 M KCl, 30 mM Tris-HCl, pH 8.0, 5 mM $MgSO_4$, 0.1 mM EGTA, and 1 mM ATP. Inorganic phosphate released was determined colorimetrically by the method of Waxman and Goldberg (1982). Protein concentrations were determined by the method of Bradford (1976) using BSA as a standard. High salt extraction routinely solubilized 80–90% of the whole axoneme ATPase activity (data not shown).

Electrophoresis

The dynein heavy chains were resolved by SDS-PAGE on a 3–5% polyacrylamide, 3–8 M urea gradient gel (Kamiya et al., 1991) using the Laemmli (1970) buffer system. For analysis of the intermediate and low molecular weight chains, a 5–15% polyacrylamide, 0–2.5 M glycerol gradient was used. All gels were stained with silver (Wray et al., 1981).

Immunological Methods

Samples of various mutants or fractions were separated on 5–15% polyacrylamide gradient gels and transferred to polyvinylidene difluoride (PVDF) membrane (0.2-mm pore size; Bio-Rad Laboratories, Richmond, CA) at 12 V for 45 min in a Genie electroblotter (Idea Scientific Co., Minneapolis, MN) in 25 mM Tris, 0.192 M glycine, and 20% methanol. After blocking in 0.1% Tween-20 and 0.2% casein in phosphate buffered saline, the blots were incubated in a 1:2,000 dilution of anti-*Volvox* actin antiserum. This antiserum was generated by immunization with the NH_2-terminal decapeptide (EEGEVSALVC) of *Volvox* actin conjugated to keyhole limpet hemocyanin and was generously provided by David Kirk (Washington University, St. Louis, MO). A 1:5,000 dilution of anti-chick brain β-tubulin antibody (Amersham Corp., Arlington Heights, IL) was also used to probe blots of whole axonemes. In both cases, immunoreactivity was detected using an alkaline phosphatase conjugated secondary antibody at a 1:10,000 dilution and the Tropix Western Light chemiluminescent detection system (Tropix, Bedford, MA). The chemiluminescent substrate was disodium 3-(4-methyloxyspiro{1,2-dioxetane-3,2′-(5′-chloro) tricyclo[3.3.1.1^{3,7}] decan}-4-yl) phenyl phosphate (CSPD). Several exposures were obtained on Kodak XRP film to ensure that the chemiluminescent signal was within the linear range. Autoradiograms were digitized for densitometry using a Javelin Ultrachip HiRes CCD camera (Javelin Electronics, Torrance, CA). Images were analyzed using the NIH-Image 1.55b software on a Macintosh LC475 computer. Control experiments indicated that signals from whole axoneme samples were linear over a range of 0.9–20 mg total protein per lane. In addition, 70% or greater of the axonemal actin was extracted by high salt treatment and observed to copurify with each inner arm subspecies in FPLC peaks *a*, *b*, *c*, *d*, *e*, and *g* (data not shown).

Electron Microscopy

Axonemes were prepared for electron microscopy as previously described (Porter et al., 1992). Briefly, axonemes were fixed with 2% glutaraldehyde, 4% tannic acid (Mallinkrodt Inc., St. Louis, MO), and 50 mM sodium phosphate at pH 6.9 for 1 h at room temperature, followed by fixation overnight in 2% glutaraldehyde and 50 mM sodium phosphate at 4°C. The samples were transferred to fresh fixative, shipped overnight express on wet ice, and then post-fixed in 1% aqueous OsO_4, dehydrated in a graded acetone series and embedded in Epon-Araldite. Sections of 60-nm nominal thickness were used for cross-sectional analysis; 40-nm sections were used for longitudinal analysis. Sections were post-stained in lead citrate and uranyl acetate and imaged at a magnification of 39,000 in a Philips CM10 microscope (Philips Electronic Instruments Co, Mahwah, NJ) operating at 80 kV.

Image Analysis

The methods for digitizing, averaging and comparing cross-sectional outer doublets are as described previously (Mastronarde et al., 1992). Approximately 50–80 outer doublets that contained protofilaments in good cross-section were selected, extracted and averaged to obtain a sample average. The images were normalized to the outer dynein arm using a program that scaled the background image intensity to zero, and the mean intensity of the region enclosing the outer arm to one. To control for inter sample variability, at least three independent preparations of each mutant strain were imaged, digitized, aligned, and averaged to obtain a sample grand average.

Cross-sections of the proximal region of the axoneme were identified by the presence of morphological markers as described by Hoops and Witman (1983). These markers included the presence of B-tubule projections in outer doublets 1, 5, and 6, and/or a two-membered cross-bridge between outer doublets 1 and 2. Outer doublets from the proximal region of the axoneme were selected, aligned, and averaged as described above. Cross-sections from axonemes that did not contain these morphological markers were pooled to obtain medial/distal averages.

Longitudinal images were selected, digitized, and averaged using the methods described in Mastronarde et al. (1992). The criteria for selecting appropriate longitudinal images included the presence of radial spokes and clear outer arms. Averages of individual axonemes were obtained by averaging at least six 96-nm radial spoke repeats. Averages from several axonemes were then combined to obtain a grand average for a particular strain. In most strains, the radial spokes repeated regularly at 96-nm intervals, but in some images of *pf3* axonemes, the arrangement of radial spokes was more irregular (data not shown). Therefore, only those regions that contain periodic radial spoke repeats were used to prepare the *pf3* averages. During the course of this study, it also came to our attention that our previously published longitudinal images (Mastronarde et al., 1992) were in fact mirror images of the true axoneme structure. To avoid possible confusion, we now display these images in their proper orientation, with the proximal end of flagella to the left and inner arm structures on the bottom.

Statistical Analysis and Difference Plots

A two-level nested analysis of variance was performed to determine the significance of variation between strains, while taking into account variation among outer doublets of the same strain (Mastronarde et al., 1992). Significant difference images were calculated to show an analysis of variance at each pixel. Differences not significant at the 0.05 confidence level were set to zero for cross-sectional averages, and differences not significant at the 0.005 confidence level for longitudinal averages.

Results

Motility Phenotypes

To assess the range of motility defects in the DRC mutants, we measured the swimming velocities of the *pf3*, *pf2*, *sup-pf-3*, and *sup-pf-4* strains and compared these values with those obtained for wild-type and inner arm mutant strains. As shown in Table I, most of the DRC mutants swim significantly slower than wild-type cells, but slightly faster than the inner arm mutant *ida4*. The motility defects are

most severe in *pf2* and *pf3*, as predicted from previous studies (Brokaw and Kamiya, 1987), but the *sup-pf-3* strain can also be readily identified by its reduced swimming velocity (~120 μm/s versus ~200 μm/s for wild-type). This decrease is consistent with estimates that the flagellar beat frequency is reduced about 15% in *sup-pf-3* strains (Brokaw and Luck, 1985). On the other hand, *sup-pf-4* cells swim at essentially wild-type velocities and are difficult to identify by simple visual examination. These differences in swimming behavior suggested that we might observe a broad spectrum of biochemical and structural phenotypes among the DRC mutant strains.

Inner Arm Dynein Isoforms in DRC Mutant Axonemes

To evaluate which inner arm isoforms might be missing in the different DRC mutants, we first prepared whole axonemes from wild-type, *pf2*, *pf3*, *sup-pf-3*, and *sup-pf-4* cells. The dynein heavy chains present in whole axonemes were then separated by SDS-PAGE on 3–5% polyacrylamide gels. While qualitative differences between strains could be observed, it was not possible to determine whether specific dynein heavy chains were simply reduced in concentration or might be missing altogether (see Fig. 3 in Porter et al., 1992; and data not shown). To resolve this question, we extracted the isolated axonemes with high salt and fractionated the dynein-containing extracts by ion exchange chromatography on a Mono-Q column. Each fraction from the profile was analyzed on both 3–5% and 5–15% polyacrylamide gradient gels to identify possible polypeptide defects. Samples representing the peak fractions from each strain can be seen in Figs. 1 and 2.

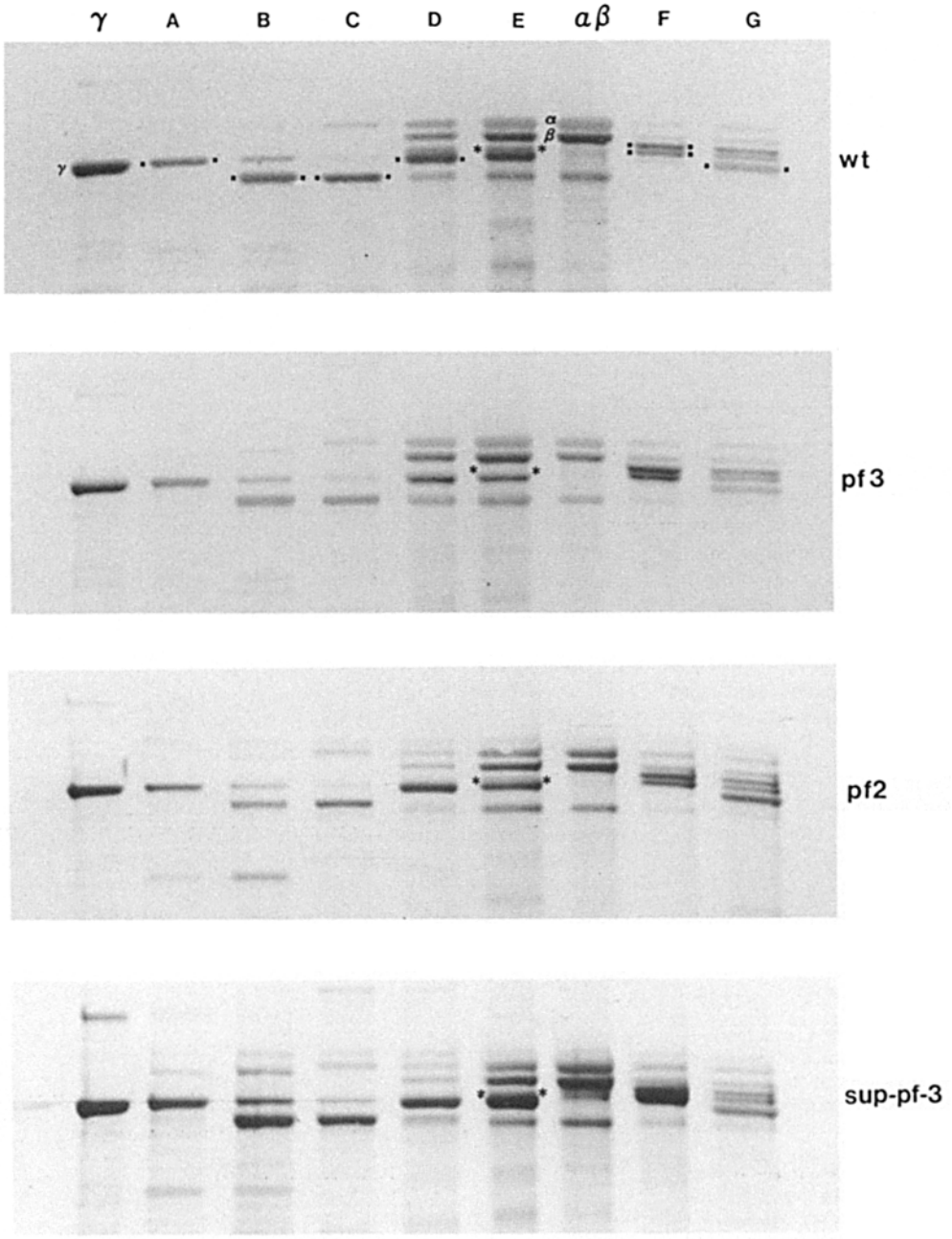

Figure 1. Dynein peaks in wild-type and DRC mutant strains. Dynein-containing extracts were fractionated by FPLC ion exchange chromatography and analyzed on 3–5% polyacrylamide gels containing a 3–8 M urea gradient. Peak fractions containing outer arm (α, β, γ) and inner arm (*A–G*) heavy chains from wild-type, *pf3*, *pf2*, and *sup-pf-3* are compared here. Because some peaks contain multiple, overlapping heavy chains, the bands corresponding to subspecies *a–g* are indicated in their respective peaks. Peaks D, E, and α/β are also loaded at a lower stoichiometry than peaks A–C. The heavy chain corresponding to subspecies *e* is marked with an asterisk in peak E. This band is visible in both peaks D and E in wild-type, but it is missing or reduced in *pf3*, *pf2* and *sup-pf-3*. Only the high molecular weight regions of the gels are shown. Silver stain.

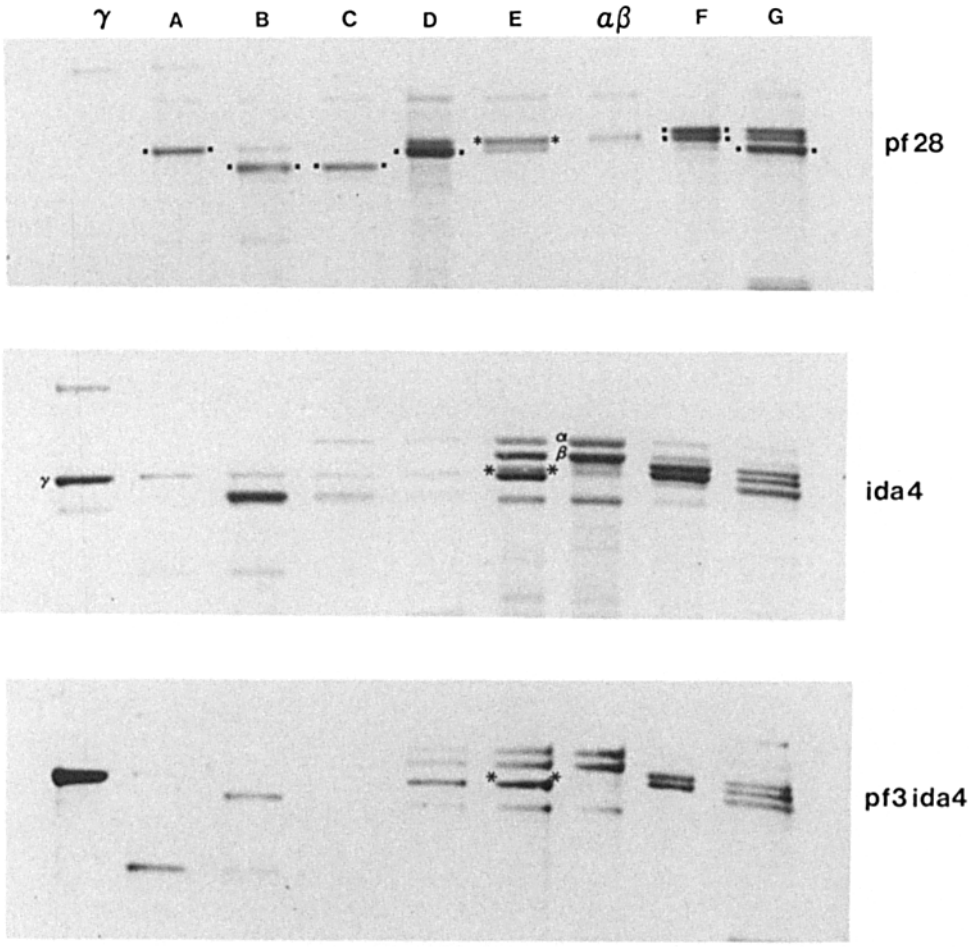

Figure 2. Dynein peaks in outer and inner arm mutant strains. Peak fractions from FPLC profiles of *pf28*, *ida4* and *pf3 ida4* were analyzed on 3–5% polyacrylamide gels containing 3–8 M urea. Fractions from *pf28* are missing the outer arm subunits but clearly show the presence of inner arm heavy chain *e*, marked with an asterisk in peak E. *ida4* is missing inner arm heavy chains *a*, *c*, and *d* as previously described (Kagami and Kamiya, 1992), while the double mutant *pf3 ida4* is missing *a*, *c*, *d*, and *e*. The band migrating at the position of band *d* in peaks A–E of the *ida4* and *pf3 ida4* profiles represents trailing γ dynein heavy chain which is not completely dissociated from the α/β outer arm complex (see also Kagami and Kamiya, 1992). Silver stain.

Fig. 1 illustrates the dynein heavy chains extracted from wild-type, *pf3*, *pf2* and *sup-pf-3* axonemes. The most striking result was the discovery that the mutant strain *pf3* completely lacks the inner arm isoform known as subspecies *e*, but retains all other inner arm dyneins. Subspecies *e* corresponds to a single dynein heavy chain that first elutes as a shoulder in peak D and peaks in E (see wild-type in Fig. 1 and *pf28* in Fig. 2). By comparison, the analysis of *pf2* profiles indicated that all inner arm isoforms are present, but some subspecies appear to be reduced relative to one another and to wild-type extracts. In particular, subspecies *e* is reduced relative to subspecies *d*, and subspecies *b* is reduced relative to subspecies *a* and *c*. Whereas subspecies *e* spans seven fractions in wild-type profiles, the *e* heavy chain is visible in only four fractions in *pf2*. This decrease is reflected in the absence of subspecies *e* from peak D and its apparent decrease in peak E (Fig. 1, third panel). A similar reduction is observed in subspecies *b*. Subspecies *b* covers six fractions in wild-type profiles, but only four fractions in *pf2*. These results were reproducible in multiple preparations, although difficult to quantify given the non-linearity of silver staining. Analysis of *sup-pf-3* profiles also shows an apparent reduction in subspecies *e*, similar to that observed with *pf2*, but the other inner arm dyneins appear present at approximately wild-type levels (Fig. 1, bottom panel).

Because subspecies *e* elutes so closely to subspecies *d*, we also constructed a *pf3 ida4* double mutant. *ida4* extracts lack the I2 subspecies *a*, *c*, and *d* (Kagami and Kamiya, 1992, and Fig. 2), and therefore a double mutant should eliminate any overlap between the D and E peaks. Consequently, the defects originating from *pf3* should be more readily identified. As shown in Fig. 2, subspecies *a*, *c*, *d*, and *e* are clearly missing in the *pf3 ida4* extracts. The faint band present in the D and E peaks is due to the incomplete separation of the γ heavy chain from the α and β heavy chains during chromatography (Kagami and Kamiya, 1992). Thus the major defect in *pf3* is the loss of subspecies *e*.

To minimize interference from outer arm heavy chains that might lead us to underestimate the inner arm defects, we also added a sucrose density gradient centrifugation step to our purification scheme and reanalyzed each mutant (see Materials and Methods). The sucrose gradient fractions containing the 23S outer arm complex were removed, and the remaining fractions were pooled and further fractionated by FPLC. Although the overall yields of protein were reduced, SDS-PAGE analysis of the resulting FPLC profiles confirmed our previous findings. Subspecies *e* is missing in *pf3* and reduced in *sup-pf-3*, but the other inner arm isoforms are still present (data not shown).

Analysis of Dynein-associated Intermediate and Light Chains

To identify dynein intermediate and light chains that might be missing in the DRC mutants, fractions from the FPLC profiles were also analyzed on 5–15% polyacrylamide gels.

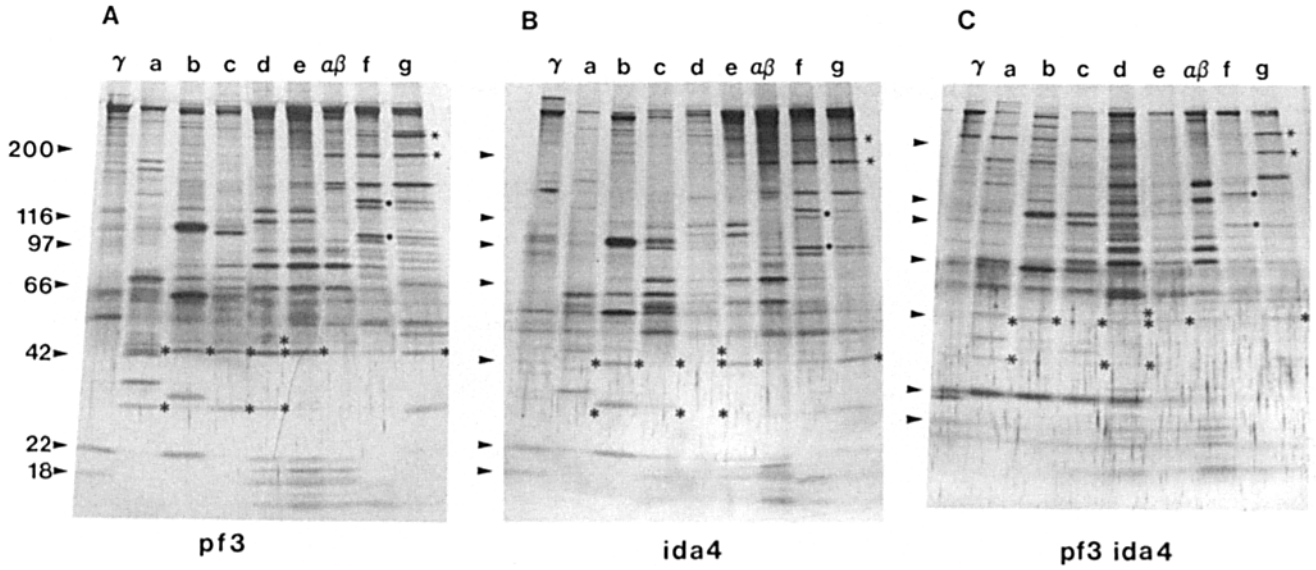

Figure 3. Intermediate and light chains associated with inner arm dynein subspecies. Peak fractions from the *pf3*, *ida4*, and *pf3 ida4* profiles were separated on 5–15% polyacrylamide gradient gels. Bands representing dynein intermediate and light chains previously identified by Kagami and Kamiya (1992) are marked. *Ida4* and *pf3 ida4* are missing the intermediate and light chains associated with I2 subspecies *a*, *c*, and *d*. The actin intermediate chain associated with subspecies *e* appears to be reduced in *pf3 ida4*. Arrowheads indicate positions of molecular weight standards. Silver stain.

In most inner arm mutants, the absence of a given heavy chain can be correlated with the loss of specific intermediate and light chain subunits. For example, in I1 mutants, the loss of the 1α and 1β heavy chains in peak F is correlated with the disappearance of the 140- and 110-kD intermediate chains associated with the I1 complex (Kagami and Kamiya, 1992; Porter et al., 1992). Likewise, the analysis of the *ida4* mutant has shown that the 42-kD actin subunit and the 28-kD light chain associated with the I2 subspecies *a*, *c*, and *d* are missing in *ida4* profiles, while the 42-kD actin subunit associated with subspecies *b*, *e*, and *g* remains (Kagami and Kamiya, 1992; and Fig. 3*b*).

In contrast to the I1 and I2 inner arm mutants, analysis of the DRC mutants indicated that the intermediate and light chains previously identified as dynein subunits are still present (Fig. 3). For example, although *pf3* lacks the heavy chain associated with subspecies *e*, a 42-kD polypeptide still elutes in the *e* region (Fig. 3 *a*). Similar results were observed with profiles obtained from *pf2* and *sup-pf-3* (data not shown). Because subspecies *e* is poorly resolved from subspecies *d*, we also examined profiles of the *pf3 ida4* strain to eliminate contaminating *d* subunits. Under these conditions, the 42-kD polypeptide eluting in the *e* region appears to be reduced, but not completely eliminated (Fig. 3 *c*).

Table II. Comparison of Biochemical and Structural Defects in DRC Mutants

Strain	FPLC defect (missing subspecies)	Relative actin concentration (% wild-type)	Inner arm intensity (% wild-type)
pf28 (oda2)	α/β, γ		
ida4-1	*a*, *c*, *d*	45.3% ± 19.5	73%
pf3	*e*	63.6% ± 15.7	63%
pf2	*e* and *b* reduced	96.4% ± 29.8	73%
sup-pf-3	*e* reduced	99.9% ± 28.5	80%
sup-pf-4	ND	93.4% ± 26.8	95%
pf3 ida4	*a*, *c*, *d*, *e*	<17%	49%

The dynein isoform defects were estimated by ion exchange chromatography of high salt extracts followed by SDS-PAGE of the complete FPLC profile (see Materials and Methods and Figs. 1 and 2). Total inner arm intensity was determined by comparison of averages of axoneme cross-sections obtained from wild-type and mutant strains and included all the regions indicated in Fig. 4*b*. Relative actin concentration was estimated by immunoblots of whole axonemes probed with anti-actin and anti-tubulin antibodies. ND, not determined.

Because of the limitations associated with analyzing intermediate and light chains on silver stained gels, we sought more quantitative estimates on the extent of the inner arm defects in the DRC mutants using an actin antibody and immunoblotting procedures (see Materials and Methods). Whole axonemes were isolated from wild-type and DRC mutant strains, separated on 5–15% polyacrylamide gels, and blotted to PVDF membranes. The blots were first probed with a *Volvox* actin antibody to determine the relative amount of actin in the different DRC mutants, and then reprobed with a tubulin antibody to control for minor differences in protein loading. The ratio of actin to tubulin was determined for each mutant and compared to that observed in wild-type (see Materials and Methods). As shown in Table II, the relative actin concentration was significantly reduced in *pf3*, *ida4*, and *pf3 ida4* axonemes, whereas the actin content of *pf2*, *sup-pf-3*, and *sup-pf-4* axonemes was not measurably different from wild-type.

Structural Defects in DRC Mutant Axonemes

In previous work, we identified a distinct structural defect in the inner arm region of *pf2* axonemes (Mastronarde et al., 1992). To determine if this defect might correspond to the location of the DRC, we analyzed axonemes from *pf3*, *sup-pf-3*, and *sup-pf-4* strains by thin section electron microscopy. At least three independent samples were prepared for each strain. Averages of the resulting cross-sectional images

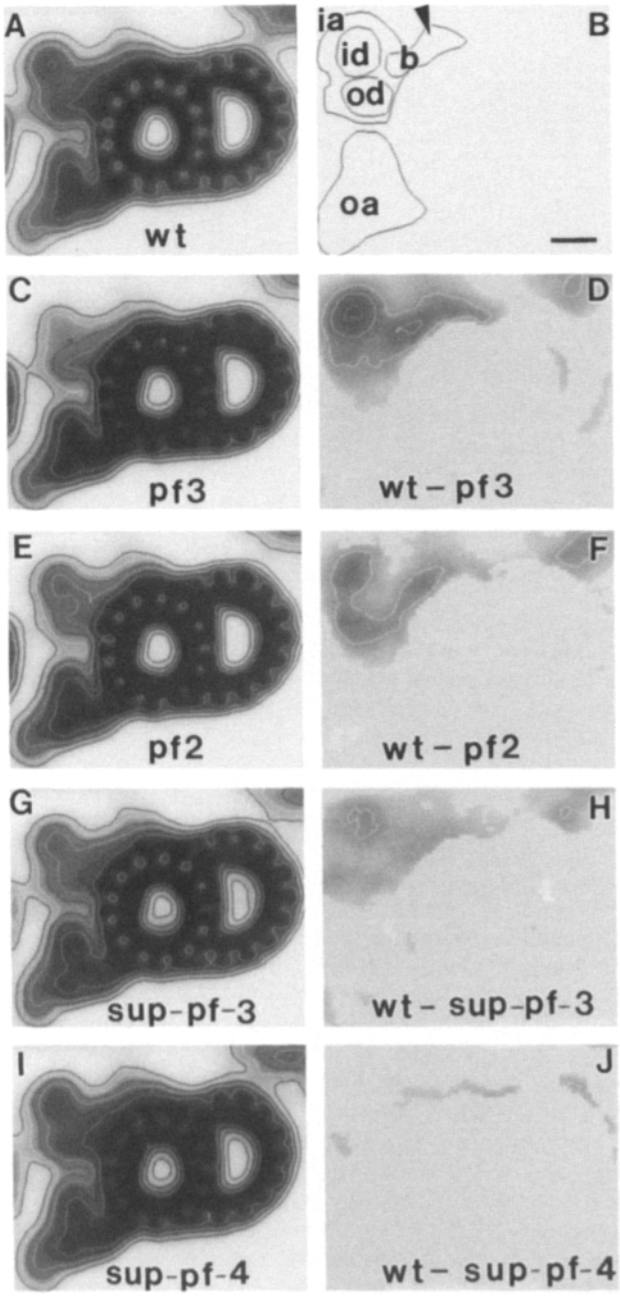

Figure 4. Grand averages and difference plots of axoneme cross-sections. (*a*) Grand average of three independent wild-type samples, containing 337 outer doublets. (*b*) Diagram of wild-type outer doublet to show areas averaged in the quantitative analysis of cross-sectional images: outer dynein arm (*oa*), inner dynein arm (*ia*), inner domain of the inner dynein arm (*id*), outer domain of the inner dynein arm (*od*), base of the inner dynein arm (*b*), arrow represents the site of radial spoke attachment. (*c* and *d*) Grand average of six *pf3* samples containing 423 doublets, and subtraction of *pf3* from wild-type. Differences not significant at the 0.05 confidence level are set to zero. (*e* and *f*) Grand average of four *pf2* samples containing 331 doublets, and subtraction of *pf2* from wild-type. (*g* and *h*) Grand average of five *sup-pf-3* samples containing 330 doublets, and subtraction of *sup-pf-3* from wild-type. (*i* and *j*) Grand average of three *sup-pf-4* samples containing 187 doublets, and subtraction of *sup-pf-4* from wild-type. Bar, 10 nm.

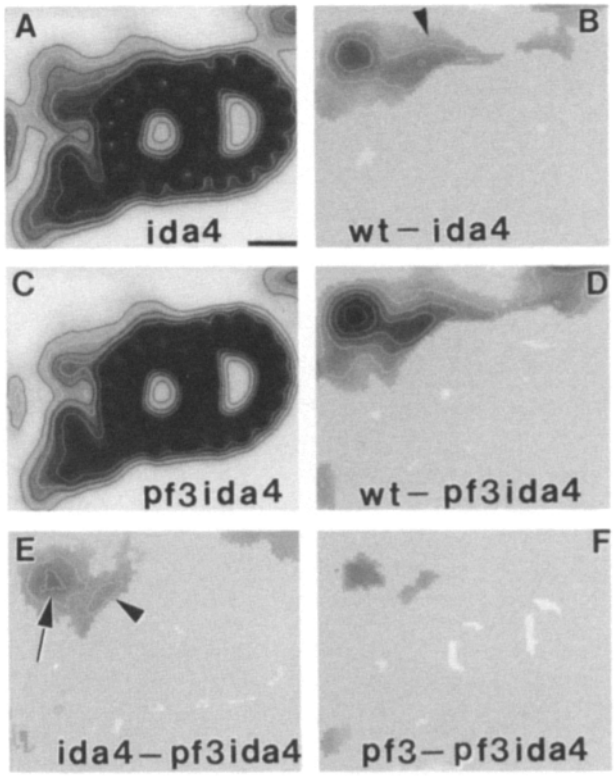

Figure 5. Grand averages and difference plots of *ida4* and *pf3 ida4* axoneme cross-sections. (*a* and *b*) Grand average of three *ida4* samples containing 223 doublets, and subtraction of *ida4* from wild-type. The arrowhead indicates the site of radial spoke attachment. (*c* and *d*) Grand average of three *pf3 ida4* samples containing 264 doublets, and subtraction of *pf3 ida4* from wild-type. (*e* and *f*) Subtraction of *pf3 ida4* from *ida4* and *pf3*, respectively. Bar, 10 nm.

are shown in Fig. 4 and can be compared with images obtained from wild-type and *pf2*. The structural defects are most clearly illustrated in the difference plots for each strain and can be further characterized with respect to the different domains of the inner arm (see Fig. 4 *b* and Materials and Methods).

As shown in Fig. 4 *c*, *pf3* axonemes have the greatest inner arm defects. The staining intensity of the inner arm region is only 63% of that seen in wild-type images (Table II), and all regions of the inner arm appear to be reduced. However, as illustrated in the difference plot (Fig. 4 *d*), the greatest defect occurs in the inner domain. This region has previously been associated with the location of the I2 inner arm isoforms which are missing in *ida4* and *pf23* axonemes (Kamiya et al., 1991; Mastronarde et al., 1992; and see below). Since *pf3* axonemes lack four components of the DRC (Huang et al., 1982; see Table I) as well as the I2 isoform known as subspecies *e* (Fig. 1), it is likely that the *pf3* defect reflects a composite view of these two structures.

The inner arm defects observed in *pf2* axonemes (Fig. 4 *e*) are less severe than those seen in *pf3*. The staining intensity of the inner arm is approximately 73% that of wild-type, and the defects are spread more evenly throughout the inner arm region (Mastronarde et al., 1992; and Fig. 4 *f*). These results are consistent with data from the FPLC profiles indicating that the dynein heavy chain defects in *pf2* are both less dramatic and slightly different from those observed in *pf3*

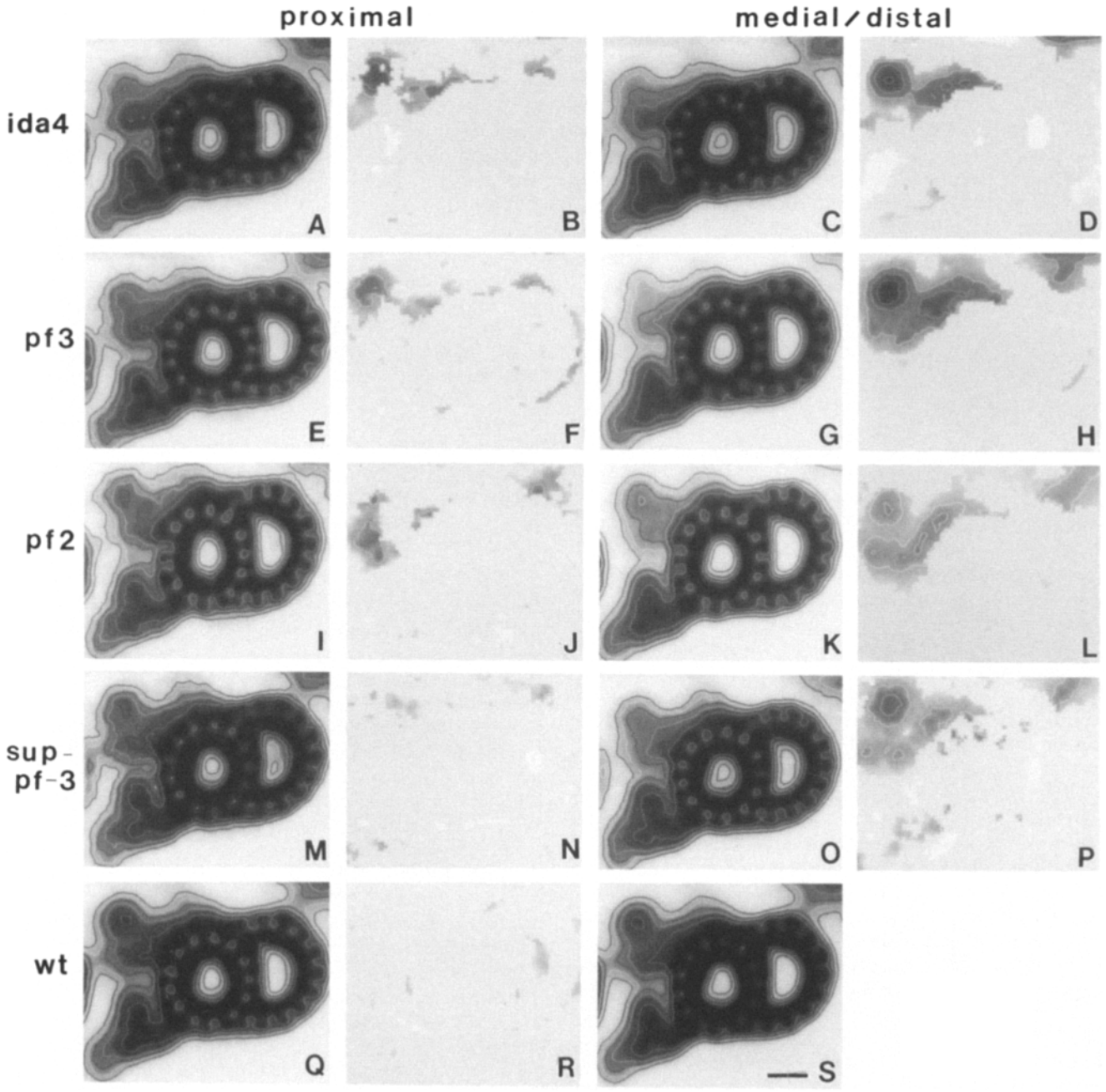

Figure 6. Grand averages of doublet cross-sections from the proximal and distal/medial regions of the axoneme. (*a*, *e*, *i*, *m*, and *q*) Proximal grand averages from *ida4*, *pf3*, *pf2*, *sup-pf-3*, and wild-type, containing 94, 80, 58, 93, and 186 doublets, respectively. (*b*, *f*, *j*, and *n*) Subtraction of proximal *ida4*, *pf3*, *pf2*, and *sup-pf-3* averages from the proximal wild-type average. Differences not significant at the 0.05 level are set to zero. (*r*) Subtraction of proximal wild-type average from medial/distal wild-type average. (*c*, *g*, *k*, *o*, and *s*) Medial/distal grand averages from *ida4*, *pf3*, *pf2*, *sup-pf-3* and wild-type, containing 170, 255, 149, 131, and 239 doublets, respectively. (*d*, *h*, *l*, and *p*) Subtraction of medial/distal averages of *ida4*, *pf3*, *pf2*, and *sup-pf-3* from the medial/distal wild-type average. Bar, 10 nm.

(Fig. 1). Since *pf2* axonemes also lack four components of the DRC, two in common with *pf3* and two others that are distinct (Huang et al., 1982; see Table I), it seems probable that similar, but not necessarily identical, structures are defective in the two strains.

Averages of *sup-pf-3* axonemes also reveal defects throughout the inner arm region (Fig. 4 *g*). *Wt - sup-pf-3* difference plots (Fig. 4 *h*) indicate that the defects are slightly less severe than those seen with *pf2*, and staining intensity of the inner arm is approximately 80% that of wild-type (Table II). These observations parallel the biochemical data indicating that *pf2* and *sup-pf-3* strains share similar deficiencies in both DRC components (Huang et al., 1982; see Table I) and the inner arm subspecies *e* (Fig. 1).

Although *sup-pf-4* axonemes lack two small DRC components (Huang et al., 1982), no significant dynein heavy chain defects have been described (Piperno et al., 1992). Likewise, electron microscopic analysis of *sup-pf-4* axonemes has failed to identify any major structural defects in the inner arm region (Fig. 4, *h* and *i*). These results indicate that total

mass of the two DRC components which are missing in *sup-pf-4* axonemes is relatively small.

To summarize, each of the DRC mutant strains, with the exception of *sup-pf-4*, shows a clear structural defect in the inner arm region of the axoneme. Moreover, the magnitude of these structural defects parallels the extent of the polypeptide defects observed in FPLC profiles of dynein extracts (Fig. 1). In addition, these defects are consistent with the deficiencies in DRC components described elsewhere (Huang et al., 1982; Piperno et al., 1992, 1994).

Comparison with Other Inner Arm Mutants

Because the major defect in *pf3* axonemes is located in the innermost region of the inner dynein arm, we decided to compare the *pf3* images with those obtained for the I2 inner arm mutant *ida4*. As expected, averages of *ida4* axonemes show major defects in the inner domain (Fig. 5 *a*; and Kamiya et al., 1991). Moreover, the difference plot between wild-type and *ida4* images further reveals that the structures corresponding to the I2 isoforms extend from the inner domain to the site of radial spoke attachment (Fig. 5 *b*, see *arrowhead*). However, although there is considerable overlap in the regions of the inner arm that are affected by the *pf3* and *ida4* mutations, the difference plots demonstrate that at least some of the structural defects are distinct (compare Figs. 4 *d* and 5 *b*).

This interpretation is also supported by the analysis of the *pf3 ida4* double mutant strain. As shown in Fig. 5 *c*, axonemes from the *pf3 ida4* mutant have greater defects than either the *pf3* or *ida4* samples, with staining intensity reduced to only 49% of wild-type levels (Table II). *Wt - pf3 ida4* difference plots show that the inner domain is particularly defective (Fig. 5 *d*), consistent with the observation that *pf3 ida4* axonemes lack four I2 isoforms (Fig. 2). Subtraction of *pf3 ida4* averages from *ida4* images reveals the approximate location of the fourth I2 isoform (subspecies *e*) in the inner domain (Fig. 5 *e*, *arrow*). The missing DRC components therefore probably correspond to a ridge of density extending from the site of radial spoke attachment through the base of the inner arm (Fig. 5 *e*, *arrowhead*). A similar density can be observed in the *wt - pf2* difference plot (Fig. 4 *f*).

However, it is important to note that the difference plot of *ida4 - pf3 ida4* (Fig. 5 *e*) is not equivalent to the difference plot of *wt - pf3* (Fig. 4 *c*), as might be expected if the mutant defects were strictly additive. Likewise, the difference plot of *pf3 - pf3 ida4* (Fig. 5 *f*) does not equal the *wt - ida4* image (Fig. 5 *b*). These results suggest that there must be some inner arm defect that is common to both mutants and/or that the mutant defects are not uniformly distributed along the length of the axonemes in both strains.

Proximal/Distal Variations in Inner Arm Structure

Because previous studies have indicated that the I2 and I3 isoforms may vary along the length of the axoneme (Piperno and Raminis, 1991), we have analyzed images of both wild-type and mutant axonemes for regional defects in inner arm structure. Cross-sections from the proximal region of the axoneme were identified by the presence of B-tubule projections and/or the presence of a crossbridge between outer doublets 1 and 2 (see Materials and Methods; and Hoops and Witman, 1983, for details). The remaining cross-sections not identified as proximal were grouped together as medial/distal in origin.

The results from this analysis are very striking and are depicted in Fig. 6. First, as shown in the *ida4* sample, some I2 inner arm defects occur throughout the length of the axoneme (Fig. 6, *a–d*). Although some variability between proximal and distal images can be observed, quantitative analysis indicates that these differences are not statistically significant. However, in all three DRC mutant strains, the defects in inner arm structure are predominantly located in the medial/distal regions of the axoneme, with only smaller (as in *pf2* and *pf3*) or even minimal (*sup-pf-3*) defects visible in proximal images (Fig. 6, *e–p*). Analysis of wild-type images detected no proximal to distal variation (Fig. 6, *q–s*).

It is interesting that the proximal defects in *pf3* and *pf2* appear to affect different regions of the inner dynein arm. The proximal defect seen in *pf3* is concentrated in the inner domain (the I2 region) and may reflect the greater defect in I2 isoforms. On the other hand, the proximal defect in *pf2* affects primarily the outer domain. This could be due to the partial deficiency of a different inner arm isoform or to the loss of a DRC component that is missing only in *pf2* (Fig. 1; and Piperno et al., 1994).

Longitudinal Analysis of Structural Defects

The inner arm structures are organized along the length of the axoneme as a complex group of at least ten different regions of density that repeat every 96 nm in register with the radial spokes (Muto et al., 1991; Mastronarde et al., 1992). To determine which inner arm structures might be altered in the DRC mutants, we obtained longitudinal images that spanned several axoneme repeats. Averages of these images were prepared, and then averages from several axonemes were combined to obtain a grand average for each strain (see Materials and Methods). The results from this analysis are shown in Fig. 7, along with grand averages of both wild-type and *pf2* axonemes for comparison. The individual structural domains are indicated as lobes 1–10 in the accompanying schematic diagram (Fig. 7 *c*).

Inspection of the grand averages for *pf3*, *pf2*, and *sup-pf-3* reveals that all three mutants share a common structural defect in a crescent-shaped domain (lobe 10) above the second radial spoke (Fig. 7, *d–f*, and arrows in 7, *g–i*). However, the difference plots indicate that the defects do vary in both shape and extent between the different strains (Fig. 7, *g–i*). Consistent with both the cross-sectional images and the biochemical data, *pf3* axonemes show the greatest defects (Fig. 7 *g*). In addition to the loss of the crescent domain (lobe 10), there are defects in lobes 5, 6, and 9, and in the second radial spoke itself. As will be shown below, the defects in lobes 5, 6, and 9 probably correspond to missing I2 isoforms, whereas the defect in lobe 10 is thought to reflect in part the location of the DRC.

Comparison of the *pf2* and *sup-pf-3* grand averages indicates that these strains are very similar in their structural defects (Fig. 7, *e* and *f*). In addition to the defect in lobe 10, both strains have small but detectable defects at the base of the second radial spoke. No obvious defects are evident in the I2 lobes, presumably because these deficiencies are too variable to appear as significantly different in the final difference plots (Fig. 7, *h* and *i*; and see discussion in Mastronarde

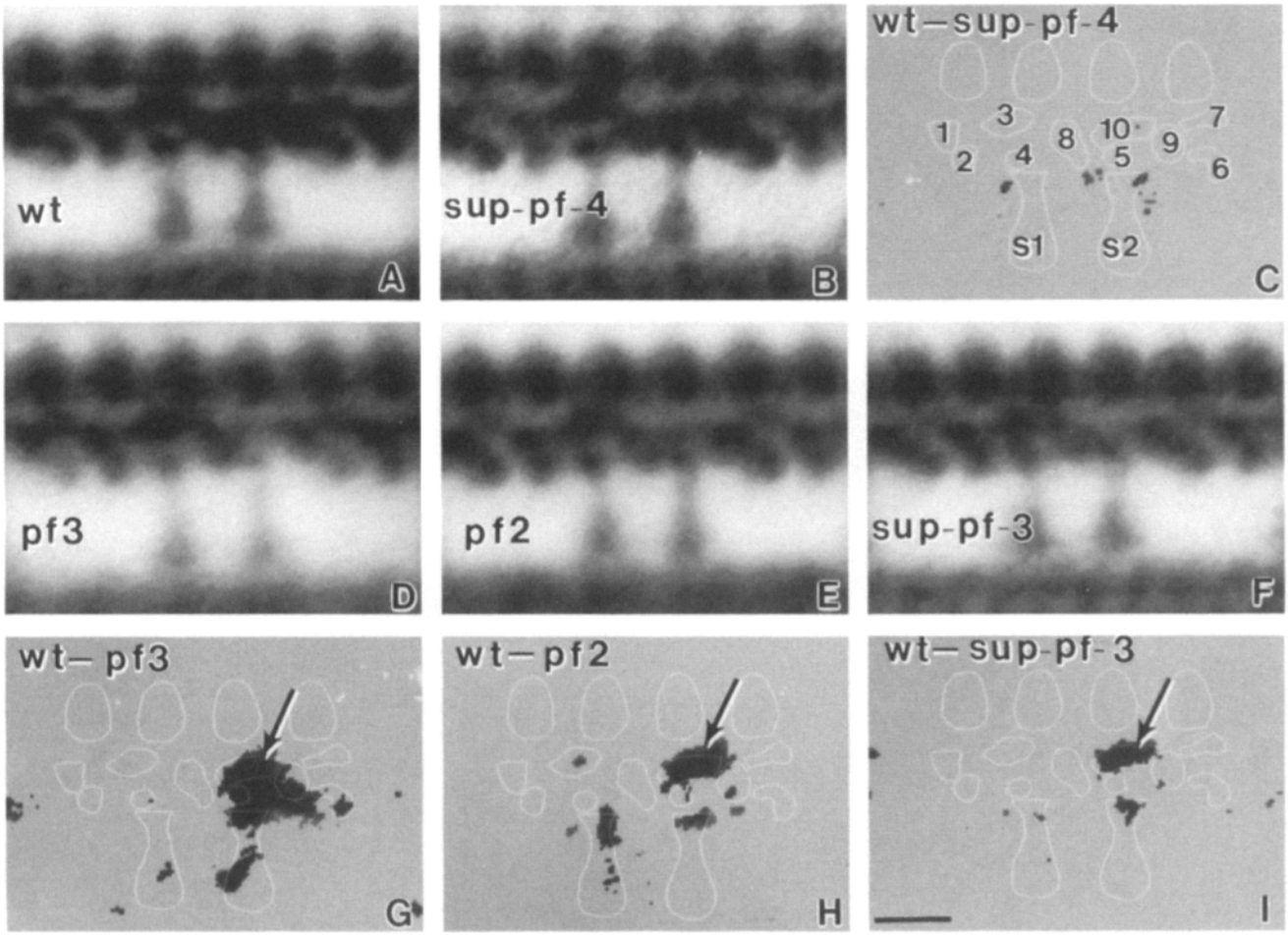

Figure 7. Analysis of longitudinal sections of wild-type and DRC mutant axonemes. (*a* and *b*) Grand averages for wild-type and *sup-pf-4*, based on 9 and 6 individual axonemes and 62 and 48 repeating units, respectively. (*c*) Difference plot between wild-type and *sup-pf-4*, with differences not significant at the 0.005 confidence level set to zero. The major lobes of density are numbered 1–10. (*d–f*) Grand averages for *pf3*, *pf2*, and *sup-pf-3* based on 7, 13, and 6 individual axonemes and 63, 98, and 44 repeating units, respectively. (*g–i*) Difference plots between wild-type and *pf3*, *pf2*, and *sup-pf-3*, respectively. The arrows indicate the defect in lobe 10 shared by these three mutants. Bar, 25 nm.

et al., 1992). As anticipated from the analysis of *sup-pf-4* in cross-section, longitudinal averages of *sup-pf-4* axonemes are not dramatically different from wild-type, although some small defects can be seen near the base of the radial spokes (Fig. 7, *b* and *c*). Although these latter defects are relatively minor, they have only been seen in averages of DRC mutant axonemes.

To further evaluate the structural relationship between the various I2 isoforms and the components of the DRC, we also analyzed images of axonemes obtained from *ida4* and *pf3 ida4* (Fig. 8). *ida4*, which lacks the three I2 isoforms *a*, *c*, and *d* (Kagami and Kamiya, 1992; and Fig. 2), is missing three distinct structures (lobes 4–6) (Mastronarde et al 1992, and Fig. 8, *a* and *b*). How the three isoforms are distributed among these three structures is still unknown, but they are clearly distinct from the crescent-shaped density (lobe 10) that is altered in the DRC mutants. However, comparison of *ida4* images with *pf3* averages reveals overlapping defects between the two strains, especially in lobes 5 and 6 (compare Fig. 8, *b* and *c*). These results suggest that *pf3* axonemes may be partially deficient in some I2 isoforms in addition to subspecies *e*.

To identify the structural defects that are unique to *pf3*, we compared the *ida4* average with that of *pf3 ida4*. Averages of *pf3 ida4* axonemes show greatly reduced inner arm structures, with major defects in lobes 4, 5, 6, 9, and 10 (Fig. 8, *d* and *e*). The only densities that remain include the I1 inner arm subunit (lobes 1–3) and portions of lobes 7, 8, and 9 (see Fig. 8 *d*). The *pf3 ida4* defects are clearly a combination of the regions shown to be affected in the original parent strains (compare Fig. 8 *e* with *b* and *c*). The difference plots highlight the probable location of many components such as the DRC and the I2 and I3 isoforms. For example, the image of *ida4* - *pf3 ida4* (Fig. 8 *f*) eliminates the three I2 isoforms in lobes 4–6 and reveals the probable location of the dynein regulatory complex (lobe 10) and the fourth I2 isoform (subspecies *e*). Subspecies *e* is likely to be represented by the tip of lobe 9 (Fig. 8, *c*, *f*, and *i*, *arrowheads*), since this lobe is uniquely missing in *pf3*. Likewise, the difference plot of *pf2* - *pf3 ida4* effectively removes the image of the DRC

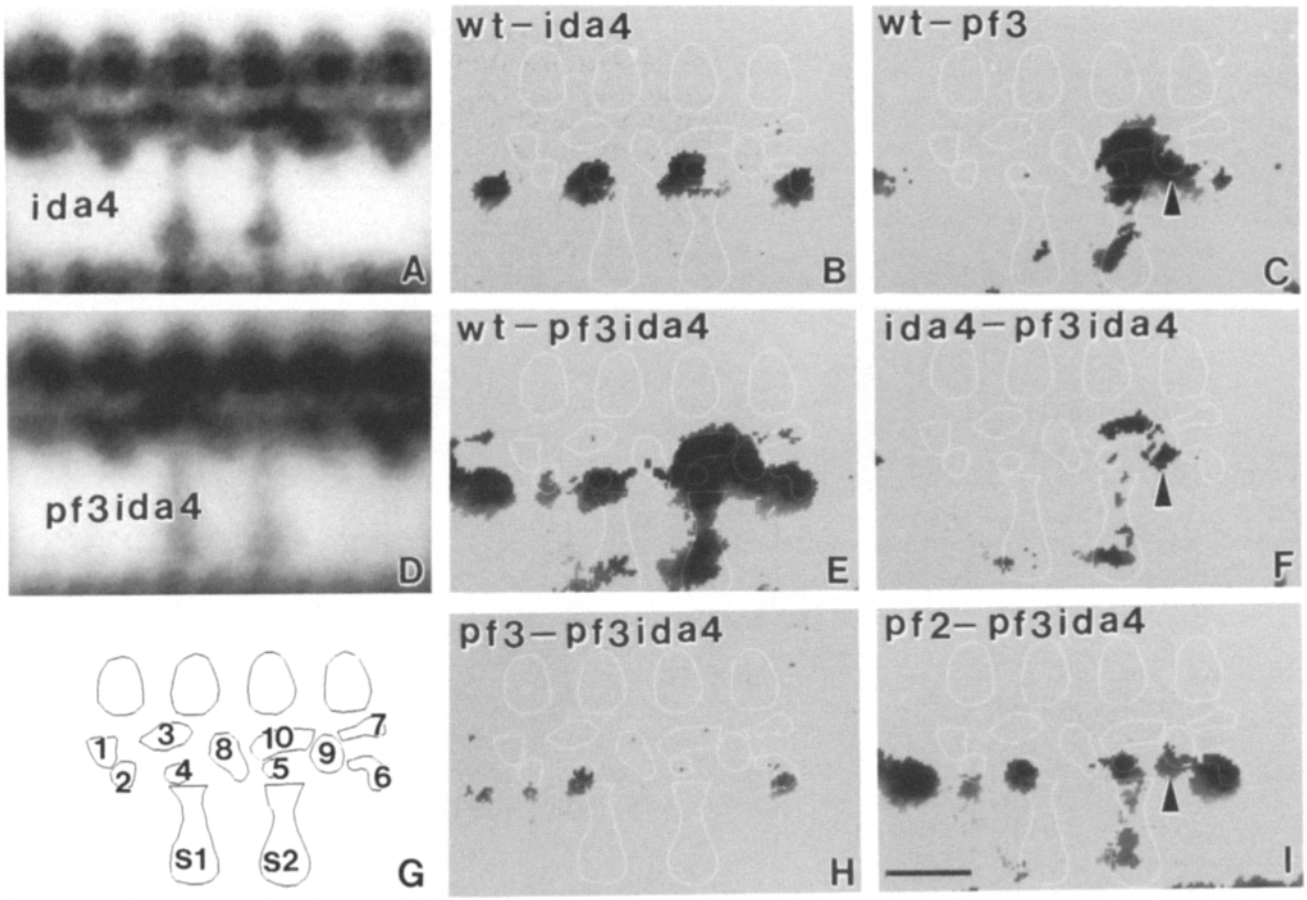

Figure 8. Analysis of longitudinal sections of axonemes missing I2 isoforms. (*a* and *d*) Grand averages for *ida4* and *pf3 ida4*, based on 5 and 12 individual axonemes and 44 and 86 repeating units. (*b*, *c*, and *e*) Difference between wild-type and *ida4*, *pf3*, and *pf3 ida4*, respectively with differences not significant at the 0.005 level set to zero. (*g*) Diagram illustrating inner arm structures relative to radial spokes 1 and 2 (S1, S2). (*f*, *h*, and *i*) Subtraction of *pf3 ida4* from *ida4*, *pf3*, and *pf2*, respectively. Bar, 25 nm.

to reveal the location of the four I2 isoforms (*a*, *c*, *d*, and *e*) as a series of four separate lobes along the inner row of the inner arm (Fig. 8 *i*). The difference plot of *pf3* - *pf3 ida4* (Fig. 8 *h*) identifies the defects that are unique to *ida4* (lobes 4 and 6) and again underscores the regions of overlap between the *ida4* and *pf3* defects (e.g., lobe 5). By default, the I3 isoforms may occupy some of the remaining unidentified domains (e.g., lobes 7, 8, or portions of lobe 9).

Discussion

In this study, we have used ion exchange chromatography and quantitative electron microscopy to characterize inner arm defects in DRC mutant strains. While chromatography enabled the separation and identification of specific dynein isoforms in each mutant, electron microscopic techniques allowed both quantitation and localization of distinct structural defects within the mutant axonemes. We have identified deficiencies in specific inner arm polypeptides in *pf3*, *pf2*, and *sup-pf-3*, and correlated these with defects in the inner arm structure. These studies indicate that a discrete subset of inner arm isoforms appears to be closely associated with certain components of the DRC. This work further suggests that some components of the DRC form a discrete structural domain located in the inner arm region.

DRC Mutants Lack Specific Inner Arm Isoforms

Three lines of evidence indicate that the primary inner arm defect in the DRC mutant axonemes is the loss of a specific I2 isoform. First, of the seven inner arm subspecies identified in dynein extracts, subspecies *e* is completely missing in *pf3* and appears to be partially reduced in *pf2* and *sup-pf-3* (Fig. 1). Second, since FPLC peaks D and E can be difficult to resolve, we confirmed the loss of subspecies *e* by analysis of the double mutant *pf3 ida4*. While *ida4* extracts lack the three I2 isoforms *a*, *c*, and *d* (Kagami and Kamiya, 1992; and Fig. 2), *pf3 ida4* extracts lack four I2 isoforms or subspecies *a*, *c*, *d*, and *e* (Fig. 2). Finally, to reduce possible interference from outer arm heavy chains, we also analyzed dynein extracts following sucrose density centrifugation to remove outer arm complexes. SDS-PAGE analysis of the resulting FPLC profiles confirmed that the primary heavy chain defect in the DRC mutants is the reduction in subspecies *e*.

The results obtained by FPLC analysis of dynein extracts are generally consistent with previous estimates of inner arm dynein defects in whole axonemes (Piperno et al., 1992; compare Tables I and II). Piperno et al. (1992) used one- and two-dimensional gels to analyze the total amounts of I2 and I3 dynein heavy chains, as well as intermediate and light chains, present in wild-type and DRC mutant axonemes. While the absolute magnitude of the estimated heavy chain

defects varies slightly between the two studies, in both cases, the mutants can be ordered with respect to their heavy chain defects as follows: *sup-pf-3* ~ *pf2* < *pf3* < *pf3 ida4* (Figs. 1 and 2; and Piperno et al., 1992). One limitation with the FPLC analysis is that it is necessary to extract the dyneins from the axoneme prior to chromatography. This step might lead us to underestimate inner arm defects if complete solubilization of the dynein arms is not achieved. This does not appear to be a major factor since ATPase measurement indicated that greater than 80–90% of the axonemal ATPase activity was extracted in each preparation. However, because it is difficult to estimate relative concentrations on silver-stained gels, we also sought more quantitative methods with which to analyze possible dynein defects.

Other experimental results indicate that there may be reductions in some of the other inner arm dynein isoforms, especially in *pf3*. First, the overlap between the structural defects observed in averages of *ida4* and *pf3* axonemes (Figs. 5 and 8) suggests that the I2 isoforms located in lobes 5 and 6 are partially reduced in *pf3*. Second, previous estimates based on densitometry of ^{35}S-labeled flagellar proteins indicate that the I2/I3 heavy chains are reduced ~47% in *pf3* axonemes relative to wild-type (Piperno et al., 1992). This decrease is larger than would be expected from the loss of a single I2 subspecies. Finally, quantitative immunoblotting procedures suggest that the actin intermediate chain which copurifies with six of the seven inner arm subspecies is reduced ~37% in *pf3* and ~55% in *ida4* (Table II). Taken together, the data indicate that while the majority of the I2 and I3 isoforms are retained in *pf3* axonemes, some subspecies (besides *e*) may be partially reduced.

Defects in the DRC do not, however, result in the destabilization of all inner arm isoforms. For instance, we see no evidence that the I1 isoform (subspecies *f*) is reduced in dynein extracts, nor have we ever observed the loss of this structure (lobes 1–3) in longitudinal sections of DRC mutant axonemes. The structure of the I1 isoform is large enough for its absence to be readily detected in individual images. Furthermore, the I1 isoform and the DRC appear to be located in different structural domains within the 96-nm axoneme repeat (see Fig. 9). Finally, reconsititution experiments with the purified I1 isoform confirm that this complex rebinds to specific sites within the axoneme distinct from the I2/I3 binding sites (Smith and Sale, 1992*b*). All of these results seem inconsistent with recent measurements indicating that I1 heavy chains are reduced in axonemes isolated from double mutant strains lacking outer arms and DRC components (e.g., *pf28 pf3*) (Piperno et al., 1994). The source of this discrepancy is unknown, but it may be related to secondary assembly defects in the double mutants, since the flagella from these recombinant strains are both shorter than wild-type and paralyzed.

DRC Mutants Lack Specific Axoneme Structures

Because the DRC is proposed to function as part of the signaling pathway between the central pair/radial spoke complex and the dynein arms (Huang et al., 1982; Piperno et al., 1994), identifying its location within the flagellar axoneme could provide important insights into possible signaling mechanisms and regulatory targets. We therefore used image averaging procedures to analyze axoneme structure in the DRC mutants. Fig. 9 summarizes our current understanding

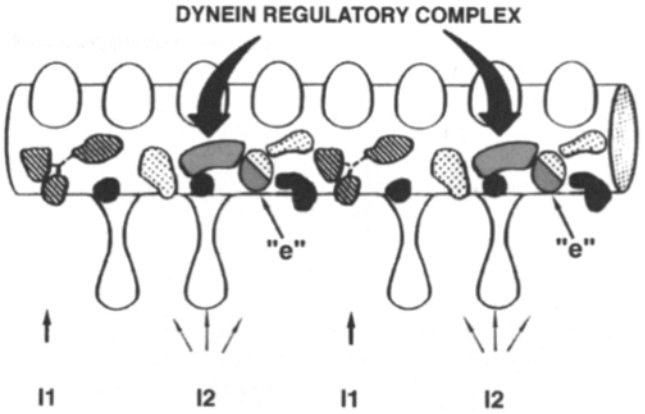

Figure 9. Summary diagram and model of inner arm organization. Our current model of structures attached to the A-tubule of the outer doublet is illustrated here, with the outer dynein arms on top, the radial spokes on the bottom, and the inner arm structures in the middle. Two 96 nm axoneme repeats are shown, with the proximal end to the left. Structural domains identified in the current study or previously in Mastronarde et al. (1992) are indicated as follows: I1 subunit, striped trilobed structure; I2 subspecies *a*, *c*, and *d*, black lobes; subspecies *e*, gray lobe; DRC, gray, crescent-shaped structure; unidentified domains, stippled lobes. Both the DRC and subspecies *e* are indicated in gray because the exact boundary between these two structures is not precisely known.

of the structural organization of inner dynein arms and their relationship to components of the DRC.

The results from the analysis of axoneme cross-sections demonstrate that the DRC mutants display a broad range of structural phenotypes, ranging from a relatively wild-type appearance in *sup-pf-4* axonemes, to decreases in inner arm intensity of 20–27% in *sup-pf-3* and *pf2*, and finally to decreases of ~37% in *pf3* (Fig. 4 and Table II). These decreases in inner arm intensity parallel the severity of inner arm defects observed in both the FPLC profiles of dynein extracts (Fig. 1) and described previously in whole axonemes (Piperno et al., 1992; see Table I). However, the magnitude of the structural defects is somewhat surprising when compared to other inner arm mutants. For example, the decreases observed in *pf3*, *pf2*, and *sup-pf-3* are similar to those previously described for *pf9* (an I1 mutant lacking two dynein heavy chains) and *ida4* (an I2 mutant lacking three dynein heavy chains) (Mastronarde et al., 1992). Closer examination of the averages clearly indicates that the *ida4*, *pf3*, and *pf3 ida4* defects are concentrated in the inner domain (the I2 region), whereas the *sup-pf-3* and *pf2* defects are more evenly distributed throughout the entire arm. Since the dynein heavy chain defects are considerably less in *pf2* and *sup-pf-3*, our interpretation of these results is that the defects in the inner domain primarily reflect reductions in I2 isoforms, whereas the defects in the outer domain indicate the probable location of the DRC.

The conclusion that defects in the inner domain are due to reductions in I2 isoforms is also consistent with the recent analysis of two newly identified inner arm mutants, *ida5* and *ida6* (Kato et al., 1993). *ida6* axonemes lack inner arm subspecies *e*, and *ida5* axonemes lack subspecies *a*, *c*, *d*, and *e* (Kato et al., 1993). In both mutants, averages of axoneme cross-sections show decreases in intensity in the innermost region of the inner dynein arm (Kato et al., 1993). These

defects are clearly similar to those observed with *pf3* and *pf3 ida4*. Whether *ida5* and/or *ida6* are also associated with defects in DRC components (or other inner arm domains) is as yet unknown. In the future, a more detailed comparison between these strains and the DRC mutants may be informative.

The proposal that certain components of the DRC are located in the inner arm region receives additional support from the analysis of DRC mutant axonemes in longitudinal view. As shown in Fig. 7, the major structural defect common to *pf3*, *pf2*, and *sup-pf-3* axonemes is the loss of a crescent-shaped density (lobe 10) located above the second radial spoke. This structure would be located in the outer domain region in cross-sectional images of the axoneme. Since the *pf3*, *pf2*, and *sup-pf-3* strains are also the most defective with respect to the loss of DRC components (Huang et al., 1982; Piperno et al., 1994), it seems likely that the crescent corresponds in part to the location of the DRC. However, it is important to consider the possibility that the loss of DRC components may also alter the distribution of other inner arm structures in this region. For instance, subspecies *e* may also contribute some density to this lobe. Additional information about the stoichiometry of the different DRC components is needed to determine if the total size of the complex is sufficient to account for the mass of the missing structure. Interestingly, recent studies by Piperno et al. (1994) suggest that the DRC may be larger than previously realized.

The longitudinal averages presented in Fig. 8 suggest that the four I2 dynein isoforms are distinct, single-headed species which are located in four separate structural domains. For example, the I2 subspecies *a*, *c*, and *d* are lost as a group of three structures (lobes 4–6) in the mutant *ida4* (Fig. 8 *b*; and Mastronarde et al., 1992). By analysis of *pf3* and *pf3 ida4*, we have now identified subspecies *e* as a fourth I2 isoform. Comparison between *ida4* and *pf3 ida4* further suggests that this isoform may occupy a portion of lobe 9 (Figs. 8, *f* and *i*, and 9). Since the I1 subunit has previously been localized to lobes 1–3 (Mastronarde et al., 1992), by default, the I3 isoforms presumably include subspecies *b* and *g* (Kagami and Kamiya, 1992) and may occupy unidentified domains such as lobes 7, 8, or remaining portions of lobe 9. The isolation and characterization of inner arm mutants specifically lacking I3 isoforms will be an important next step toward the identification of the remaining domains within the longitudinal images, allowing further refinements of the model to be made.

The position of the *e* subspecies directly adjacent to the radial spokes and the DRC suggests that this isoform may play an important role in the response to signals from the central pair/radial spoke complex. Indeed, the motility phenotypes of mutants lacking the *e* subspecies indicate that it does contribute to both the generation of an asymmetric flagellar waveform and efficient forward motility (Brokaw and Kamiya, 1987; Kato et al., 1993; and Table I). Moreover, the observation that the structural defects in the DRC mutants vary along the length of the axoneme (Fig. 6) suggests that the *e* subspecies may be located primarily in the medial/distal region of the axoneme. In the future, it will be important to reexamine this hypothesis with other *e* deficient strains (such as *ida6*) or with dynein isoform specific antibodies. It would also be of interest to identify those axoneme components responsible for targeting inner arm isoforms to their specific locations. These may include polypeptide subunits unique to each isoform and/or specific binding sites associated with different components of the DRC.

Functions of DRC Components

One of the major implications from the current work and the recent study of Piperno et al. (1994) is that the various components of the DRC perform different functions in the coordination of dynein activity. Some may serve primarily to regulate activity, while others appear to facilitate the attachment of specific dynein isoforms to their proper axoneme location. For example, DRC components 5 and 6 are deficient in all the DRC mutants identified (Huang et al., 1982; Piperno et al., 1992, 1994). Since the loss of these two polypeptides in the *sup-pf-4* mutant is sufficient to restore flagellar motility to central pair/radial spoke defective strains, DRC components 5 and 6 may be the primary polypeptides that modify dynein activity in situ (Huang et al., 1982; Piperno et al., 1994). It would therefore be interesting to determine if the absence of DRC components 5 and 6 can either increase microtubule sliding velocities and/or alter phosphorylation states in radial spoke defective axonemes, as might be predicted from the work of Smith and Sale (1992*a*).

The inner arm defects observed in *pf3*, *pf2*, and *sup-pf-3* suggest that the other DRC components play a role in mediating structural interactions between the dynein arms, the A-tubule of the outer doublet, and the radial spokes. For instance, *pf2* and *sup-pf-3* mutants share overlapping deficiencies in DRC components 3–7 (Huang et al., 1982; Piperno et al., 1992, 1994) and defects of similar magnitude in inner arm isoforms (Fig. 1; and Piperno et al., 1992) and inner arm structure (Figs. 4 and 7; and Table II). On the other hand, *pf3* mutants lack DRC components 1–2 and 5–6 (Huang et al., 1982) and are the most defective with respect to assembly of both radial spoke and inner arm structures (Figs. 4 and 7). Thus, DRC components 3, 4, and 7 may stabilize the binding of inner arm isoforms, whereas components 1 and 2 may actually form part of the binding site for both radial spokes and certain inner arm subspecies. This interpretation is consistent with both our structural observations and the recent rebinding experiments of Piperno et al. (1994). Further insight into the function of the various DRC components will require the isolation and characterization of each polypeptide in the complex.

Conclusions

The characterization of the DRC mutant strains, several of which possess inner arm defects, has provided several new insights into the organization and function of the dynein regulatory complex. First, this study extends previous work indicating that inner arm isoforms bind to specific sites on the outer doublet microtubule (Smith and Sale, 1992*b*; Mastronarde et al., 1992) by identifying the positions of several inner arm subspecies. Second, our structural analyses have also identified a discrete structural domain as the likely location of the DRC. Positioned between the radial spokes and the inner and outer dynein arms, this structure is ideally situated to mediate signals, either mechanical, enzymatic, or both, between different axoneme components. This structure also provides the first piece of direct evidence indicating that the various components of the DRC are physically associated

with one another. Finally, the close physical relationship between this structure and certain inner arm isoforms is consistent with the proposal that the DRC also acts as an adapter that binds these isoforms to the outer doublet (Piperno et al., 1994). Given the overall conservation in the structural organization of the dyneins, this function of the DRC may be analogous to that of other regulatory complexes that are thought to facilitate the binding of cytoplasmic dyneins to their various cellular cargoes (Schroer and Sheetz, 1991). Further analysis of the DRC mutants by in vitro assays and by the characterization of individual DRC components should provide additional insights into the nature of the regulatory signals that coordinate dynein activity and generate flagellar motility.

M. E. Porter would like to thank Paul Matsudaira for his suggestions on the display of longitudinal images and Tom Hays for comments on the manuscript.

This work was supported by National Science Foundation grants to M. E. Porter (DCB-9005079 and MCB-9305217) and a National Institutes of Health Biotechnology Resource grant (No. RR0592) to the Laboratory for Three-Dimensional Microscopy (University of Colorado, Boulder, CO, J. R. McIntosh, director). L. C. Gardner and C. A. Perrone were also supported in part by a research training grant (BIR-9113444) for Interdisciplinary Studies on the Cytoskeleton from the National Science Foundation. Additional support to M. E. Porter was provided by the Minnesota Medical Foundation and the Mcknight-Land Grant Professorship. This work was also aided in part by a Basil O'Connor Starter Scholar Research Award No. 5-FY91-0607 from the March of Dimes Birth Defects Foundation.

Received for publication 27 July 1994 and in revised form 7 September 1994.

References

Bradford, M. 1976. A rapid and sensitive method for quantitation of microgram quantities of proteins utilizing the principle of protein-dye binding. *Anal. Biochem.* 72:248–284.

Brokaw, C. J., D. J. L. Luck, and B. Huang. 1982. Analysis of the movement of *Chlamydomonas* flagella: the function of the radial spoke system is revealed by comparison of wild-type and mutant flagella. *J. Cell Biol.* 92: 722–732.

Brokaw, C. J., and R. Kamiya. 1987. Bending patterns of *Chlamydomonas* flagella: IV. Mutants with defects in inner and outer dynein arms indicate differences in dynein arm function. *Cell Motil. Cytoskeleton.* 8:68–75.

Brokaw, C. J., and D. J. L. Luck. 1985. Bending patterns of *Chlamydomonas* flagella. III. A radial spoke head deficient mutant and a central pair deficient mutant. *Cell Motil. Cytoskeleton.* 5:195–208.

Fox, L. A., and W. S. Sale. 1987. Direction of force generated by the inner row of dynein arms on flagellar microtubules. *J. Cell Biol.* 105:1781–1787.

Goodenough, U., and J. Heuser. 1984. Structural comparison of purified dynein proteins with in situ dynein arms. *J. Mol. Biol.* 180:1083–1118.

Goodenough, U. W., and J. E. Heuser. 1989. Structure of the soluble and in situ ciliary dyneins visualized by quick-freeze deep-etch microscopy. In Cell Movement. Vol. 1., F. D. Warner, P. Satir, and I. R. Gibbons, editors. Alan R. Liss, Inc., New York. 121–140.

Goodenough, U. W., B. Gebhart, V. Mermall, D. R. Mitchell, and J. E. Heuser. 1987. High pressure liquid chromatography fractionation of *Chlamydomonas* dynein extracts and characterization of inner-arm dynein subunits. *J. Mol. Biol.* 194:481–494.

Holmes, J. A., and S. K. Dutcher. 1989. Cellular asymmetry in *Chlamydomonas reinhardtii*. *J. Cell Sci.* 94:273–285.

Hoops, H. J., and G. B. Witman. 1983. Outer doublet heterogeneity reveals structural polarity related to beat direction in *Chlamydomonas* flagella. *J. Cell Biol.* 97:902–908.

Huang, B., G. Piperno, and D. J. L. Luck. 1979. Paralyzed flagella mutants of *Chlamydomonas reinhardtii* defective for axonemal doublet microtubule arms. *J. Biol. Chem.* 254:3091–3099.

Huang, B., Z. Ramanis, and D. J. L. Luck. 1982. Suppressor mutations in *Chlamydomonas* reveal a regulatory mechanism for flagellar function. *Cell.* 28:115–124.

Kagami, O., and R. Kamiya. 1992. Translocation and rotation of microtubules caused by multiple species of *Chlamydomonas* inner-arm dynein. *J. Cell Sci.* 103:653–664.

Kamiya, R. 1988. Mutations at twelve independent loci result in absence of outer dynein arms in *Chlamydomonas reinhardtii*. *J. Cell Biol.* 107:2253–2258.

Kamiya, R., E. Kurimoto, and E. Muto. 1991. Two types of *Chlamydomonas* flagellar mutants missing different components of inner-arm dynein. *J. Cell Biol.* 112:441–447.

Kato, T., O. Kagami, T. Yagi, and R. Kamiya. 1993. Isolation of two species of *Chlamydomonas reinhardtii* flagellar mutants, *ida5* and *ida6*, that lack a newly identified heavy chain of the inner dynein arm. *Cell Struct. Func.* 18:371–377.

King, S. M., T. Otter, and G. B. Witman. 1986. Purification and characterization of *Chlamydomonas* flagellar dyneins. *Methods Enzymol.* 134:291–306.

Kurimoto, E., and R. Kamiya. 1991. Microtubule sliding in flagellar axonemes missing inner- or outer-arm dynein: velocity measurements on new types of mutants by an improved method. *Cell Motility Cytoskeleton.* 19:275–281.

Laemmli, U. K. 1970. Cleavage of structural proteins during the assembly of the head of bacteriophage T4. *Nature (Lond.).* 227:680–685.

Luck, D. J. L., and G. Piperno. 1989. Dynein arm mutants of *Chlamydomonas*. *In*: Cell Movement. Vol. 1. F. D. Warner, P. Satir, and I. R. Gibbons, editors, Alan R. Liss, Inc., New York. 49–60.

Luck, D. J. L., G. Piperno, Z. Ramanis, and B. Huang. 1977. Flagellar mutants of *Chlamydomonas*: study of radial spoke-defective strains by dikaryon and revertant analysis. *Proc. Natl. Acad. Sci. USA.* 74:3456–3460.

Mastronarde, D. N., E. T. O'Toole, K. L. McDonald, J. R. McIntosh, and M. E. Porter. 1992. Arrangement of inner dynein arms in wild-type and mutant flagella of *Chlamydomonas*. *J. Cell Biol.* 118:1145–1162.

Mitchell, D. R., and J. L. Rosenbaum. 1985. A motile *Chlamydomonas* flagellar mutant that lacks outer dynein arms. *J. Cell Biol.* 100:1228–1234.

Muto, E., R. Kamiya, and S. Tsukita. 1991. Double-rowed organization of inner dynein arms in *Chlamydomonas* flagella revealed by tilt series, thin-section electron microscopy. *J. Cell Sci.* 99:57–66.

Piperno, G., and D. J. L. Luck. 1979. Axonemal adenosine triphosphatases from flagella of *Chlamydomonas reinhardtii*. *J. Biol. Chem.* 254:3084–3090.

Piperno, G., and Z. Ramanis. 1991. The proximal portion of *Chlamydomonas* flagella contains a distinct set of inner dynein arms. *J. Cell Biol.* 112: 701–709.

Piperno, G., K. Mead., and W. Shestak. 1992. The inner dynein arms I2 interact with a "dynein regulatory complex" in *Chlamydomonas* flagella. *J. Cell Biol.* 118:1455–1463.

Piperno, G., K. Mead, M. LeDizet, and A. Moscatelli. 1994. Mutations in the "dynein regulatory complex" alter the ATP-insensitive binding sites for inner arm dyneins in *Chlamydomonas* axonemes. *J. Cell Biol.* 125:1109–1117.

Piperno, G., Z. Ramanis, E. F. Smith, and W. S. Sale. 1990. Three distinct inner dynein arms in *Chlamydomonas* flagella: molecular composition and location in the axoneme. *J. Cell Biol.* 110:379–389.

Porter, M. E., J. Power, and S. K. Dutcher. 1992. Extragenic suppressors of paralyzed flagellar mutations in *Chlamydomonas reinhardtii* identify loci that alter the inner dynein arms. *J. Cell Biol.* 118:1163–1176.

Sager, R., and S. Granick. 1953. Nutritional studies with *Chlamydomonas reinhardtii*. *Annu. NY Acad. Sci.* 466:18–30.

Sale, W. S., and P. Satir. 1977. The direction of active sliding of microtubules in *Tetrahymena* cilia. *Proc. Natl. Acad. Sci. USA.* 74:2045–2049.

Schroer, T. A., and M. P. Sheetz. 1991. Two activators of microtubule-based vesicle transport. *J. Cell Biol.* 115:1309–1318.

Smith, E. F., and W. S. Sale. 1991. Microtubule binding and translocation by inner dynein arm subtype I1. *Cell Motil. Cytoskeleton.* 18:258–268.

Smith, E. F., and Sale, W. S. 1992*a*. Regulation of dynein-driven microtubule sliding by the radial spokes in flagella. *Science (Wash. DC).* 257:1557–1559.

Smith, E. F., and W. S. Sale. 1992*b*. Structural and functional reconstitution of inner dynein arms in *Chlamydomonas* flagellar axonemes. *J. Cell Biol.* 117:573–581.

Smith, E. F., and W. S. Sale. 1994. Mechanisms of flagellar movement: functional interactions between dynein arms and the radial spoke-central apparatus complex. *In* Microtubules. J. Hyams and C. Lloyd, editors. Wiley-Liss, Inc., New York, NY. 381–392.

Takada, S., H. Sakakibara, and R. Kamiya. 1992. Three-headed outer arm dynein from *Chlamydomonas* that can functionally combine with outer-arm-missing axonemes. *J. Biochem.* 111:758–762.

Waxman, L., and A. Goldberg. 1982. Protease La from *Escherichia coli* hydrolyzes ATP in a linked fashion. *Proc. Natl. Acad. Sci. USA.* 79:4883–4887.

Witman, G. B. 1986. Isolation of *Chlamydomonas* flagella and flagellar axonemes. *Methods Enzymol.* 134:280–290.

Witman, G. B., J. Plummer, and G. Sander. 1978. *Chlamydomonas* flagellar mutants lacking radial spokes and central tubules. Structure and function of specific axonemal components. *J. Cell Biol.* 76:729–747.

Witman, G. B., K. A. Johnson, K. K. Pfister, and J. S. Wall. 1983. Fine structure and molecular weight of the outer arm dyneins of *Chlamydomonas*. *J. Submicrosc. Cytol.* 15:193–198.

Wray, W., T. Boulikas, V. P. Wray, and R. Hancock. 1982. Silver staining of proteins in polyacrylamide gels. *Anal. Biochem.* 118:197–203.